ISSN 1063-7788, Physics of Atomic Nuclei, 2020, Vol. 83, No. 10, pp. 1–11. © Pleiades Publishing, Ltd., 2020.
Russian Text © The Author(s), 00000, published in Yadernaya Fizika i Inzhiniring, 00000, Vol. 00000, No. 00000, pp. 00000–00000.

Atom Probe Analysis of High-Entropy Alloy AlCoCrFeNi

S. V. Rogozhkin[a,b], A. S. Shutov[a,*], A. A. Khomich[a], A. A Nikitin[a,b], A. A. Lukyanchuk[a], O. A. Raznitsyn[a], and L. Meshi[c]

[a] *Alikhanov Institute for Theoretical and Experimental Physics, National Research Center Kurchatov Institute, Moscow, 117218 Russia*

[b] *National Research Nuclear University MEPhI (Moscow Engineering Physics Institute), Moscow, 115409 Russia*

[c] *Department of Materials Engineering, Ben Gurion University of the Negev, Beer-Sheva, Israel*

**e-mail: Anton.Shutov@itep.ru*

Received October 18, 2018; revised December 24, 2018; accepted February 15, 2019

Abstract—In this paper, the results of study of the AlCoCrFeNi high-entropy alloy by means of atom probe tomography are presented. Two phases were found, one enriched in Fe and Cr and the other enriched in Ni and Al. Owing to the complex surface morphology and spatial configuration of the phases, they were analyzed by various statistical methods. The Fe–Cr phase has a honeycomb structure that contains Co particles with the characteristic size of the order of 10 nm. The enrichment of the cell boundaries in Fe and Cr atoms reaches 50 at %. In turn, the Al–Ni phase is enriched in each of these elements up to 30 at % and contains nanoscale precipitates of Fe and Cr atoms. The volume density of these clusters is ~6×10^{17} cm^{-3}.

Keywords: atom probe tomography, data reconstruction algorithm, high-entropy alloys

DOI: 10.1134/S106377882010021X

INTRODUCTION

Materials of a new class of high-entropy alloys (HEA) [1, 2] consisting of four or more metal elements with almost equiatomic concentration demonstrate unique properties and differ fundamentally in many aspects from conventional alloys with one or two base elements. HEAs have the potential to be used in extreme or special environments owing to both the improvement of traditional properties and the implementation of new specific combined properties. The creation of HEAs also addresses a number of new fundamental issues in materials science. The unique properties of HEAs, namely, high specific entropy [1, 3], slow diffusion [3, 4], and strong lattice distortion [3, 5], are expected to improve the stability of phases and microstructure as a whole and, as a result, improve the stability of mechanical properties. HEAs have demonstrated impressive radiation resistance. Such results make these materials attractive for nuclear engineering applications [6].

The Cantor equiatomic alloy CoCrFeMnNi exhibits both high plasticity [7, 8], tensile strength [9, 10], and high fracture resistance at low temperatures [8, 10]. Al0.5CoCrCuFeNi alloy has high fatigue resistance [11], and CoCrFeNiTi and AlCoCrFeNiTi alloys display high durability [12].

In the literature, AlCoCrCuFeNi alloy demonstrating high mechanical properties has been studied in detail [13, 14]. Most of the phases of AlCoCrCuFeNi equiatomic alloy are enriched in Al–Ni and Cr-Fe with BCC structures, while the phase enriched in Al–Ni is an ordered phase of the B2 type, and the phase enriched in Cr-Fe is an unordered phase [15]. In order to exclude formation of phases enriched in Cu at the boundaries and inside the grains, and to decrease the number of phases, this element was excluded from the new alloys of the AlCoCrFeNi type [16–19]. In [18], it was shown that AlCoCrFeNi alloy solidified forming dendrites and interdendrites, inside which two or three phases were detected.

In [20], it was shown that the B2 matrix of the dendrite (DR) and interdendrite (ID) regions in the studied AlCoCrFeNi alloy contained domains with different orders. In the ID region, a short-range order of domains was observed, while in the DR region, the domains had a long-range order with the modulation vector of 1/5[110]. Assessment of strain in the particle/matrix interface indicated the cessation of growth of the particles in the DR area.

The purpose of this work is to analyze in detail the chemical composition of phases of AlCoCrFeNi alloy using atom probe tomography in order to study the distribution of chemical elements at phase boundaries and their significance in the process of forming the nanostructure of the material. In addition, the efficiency of various methods of statistical processing of atom probe tomography data with regard to the analysis of nanoscale phases with complex spatial configuration is demonstrated.

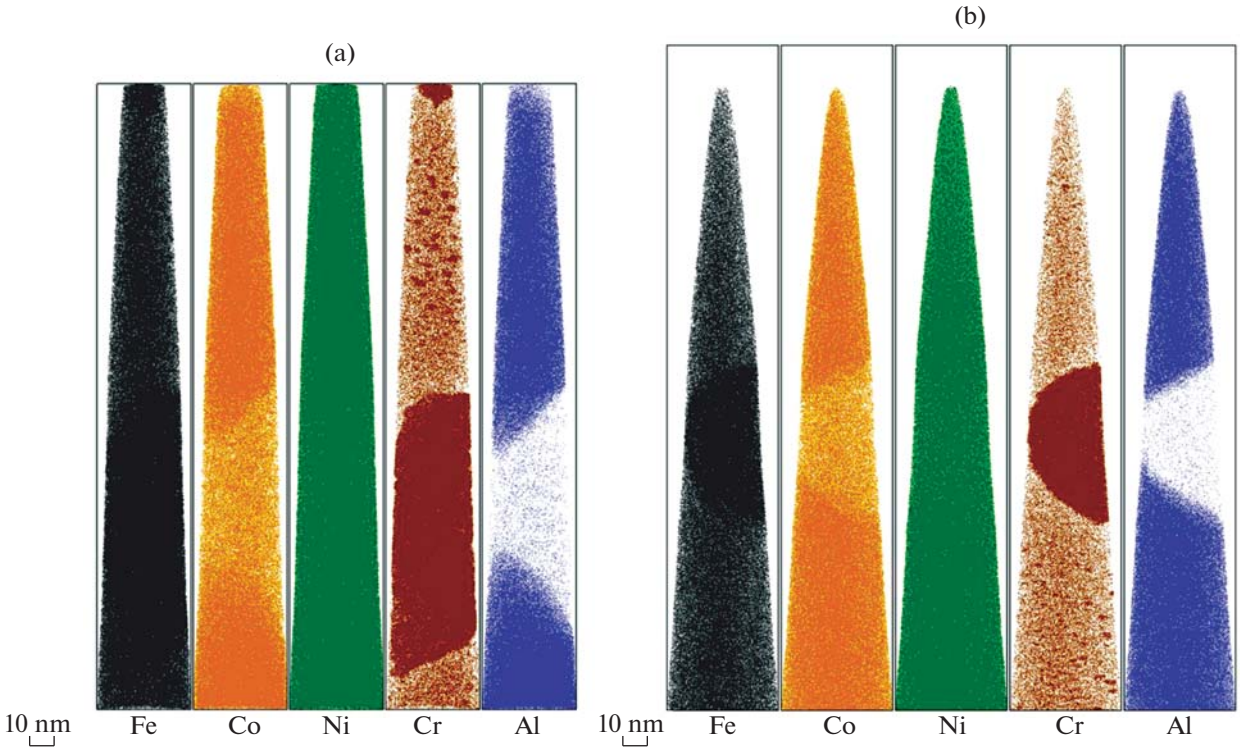

Fig. 1. Examples of the AlCoCrCuFeNi HEA atomic maps. For illustrative purposes, 10% of detected atoms are shown.

1. MATERIALS AND METHODS

AlCoCrFeNi alloy with an equiatomic element ratio was cast (see [20]) of 99.9% pure components of the alloy in a vacuum arc furnace in a purified Ar atmosphere. The castings were disks 30 mm in diameter and 13 mm in height. The melting was repeated five times. The castings were turned over between the meltings to improve the chemical homogeneity. The melt was left for solidification in a water-cooled copper crucible for crystallization.

In order to prepare the specimens for atomic-probe tomography, workpieces with the sizes of 0.3 × 0.3 × 10 mm were made of the initial alloy by the method of electroerosion cutting in water. This method does not create stresses in the process of specimen preparation and thus does not lead to any volumetric changes, as opposed to mechanical cutting methods. In addition, the presence of water and the features of the method prevent the specimen from being heated above 100ºC. Further thinning of the workpieces was carried out using standard methods of electrochemical anode electropolishing to form the specimen tip with the radius of curvature of 15–50 nm and the rate of taper of the needle specimen less than 0.1. The obtained needle specimens were controlled using a JEOL 1200 EX transmission electron microscope.

In order to study the distribution of chemical elements in the structural components of the alloy, an atom probe tomograph with femtosecond laser assisted evaporation (APPLE-3D) developed at the Alikhanov Institute for Theoretical and Experimental Physics, National Research Center Kurchatov Institute, was used [21]. In the study, a DLD80 delay line detector was used with the detection efficiency of ~90%. The 3D reconstruction of the atom arrangement inside the specimen was performed by special KVANTM-3D software [22].

The presented data was obtained at the constant voltage of 2–9 kV in the specimen, laser pulse duration of 300 fs, laser pulse frequency of 25 kHz, laser power of ~11 mW, harmonic of 515 nm, specimen temperature of 50 K, and vacuum in the process of study at the level of (5–7) × 10^{-10} Torr. The mean evaporation intensity was 5 atoms per 1000 laser pulses. The data

Table 1. Chemical composition of the phases enriched in Fe, Cr or Al, Ni of the AlCoCrFeNi high-entropy alloy (at %)

Element	Fe	Cr	Ni	Al	Co
Fe–Cr phase	32.1 ± 0.1	41.3 ± 0.1	11.0 ± 0.1	0.6 ± 0.1	15.1 ± 0.1
Al–Ni phase	20.3 ± 0.1	7.1 ± 0.1	28.1 ± 0.1	24.8 ± 0.1	19.9 ± 0.1

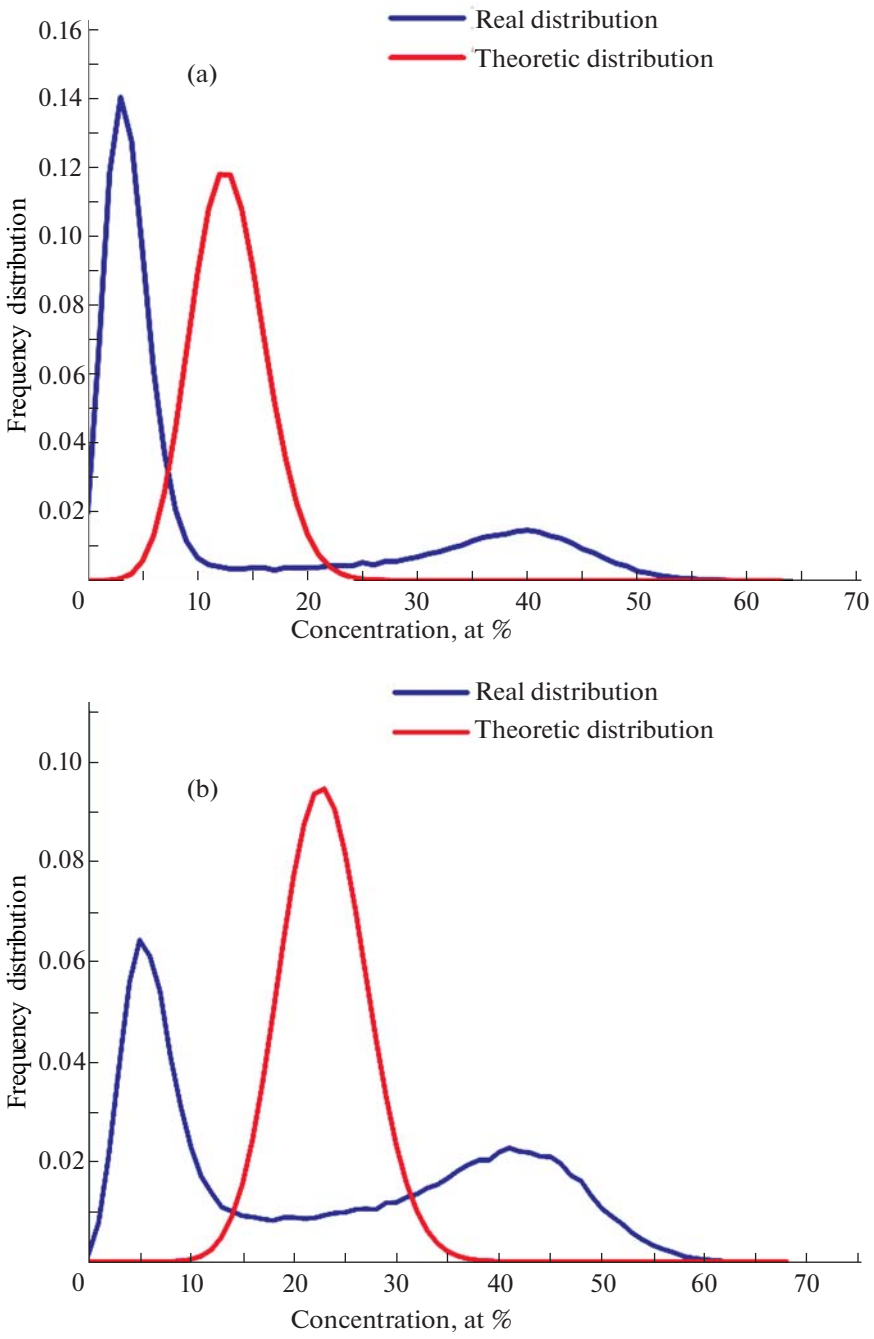

Fig. 2. Frequency distributions of chromium in the studied volumes of AlCoCrFeNi HEA presented in Figs. 1A and 1B, respectively.

collection conditions were optimized in the same way as described in [23].

A wide range of methods is used to analyze atom probe data [24]. Atomic maps or their parts are used for visualization of the examined volumes. In addition, other methods of material characterization are used: the frequency distributions of elements, the nearest neighbor method, the method of pair-correlation functions, the method of local chemical enrich-

Table 2. Chemical composition of the matrix and inclusions in the Fe–Cr phase (at %)

Element	Fe	Cr	Ni	Al	Co
Matrix	31 ± 1	43 ± 2	14 ± 1	0.6 ± 0.2	13.9 ± 0.9
Co–Fe particles	48 ± 4	4 ± 3	20 ± 3	2 ± 1	26 ± 3

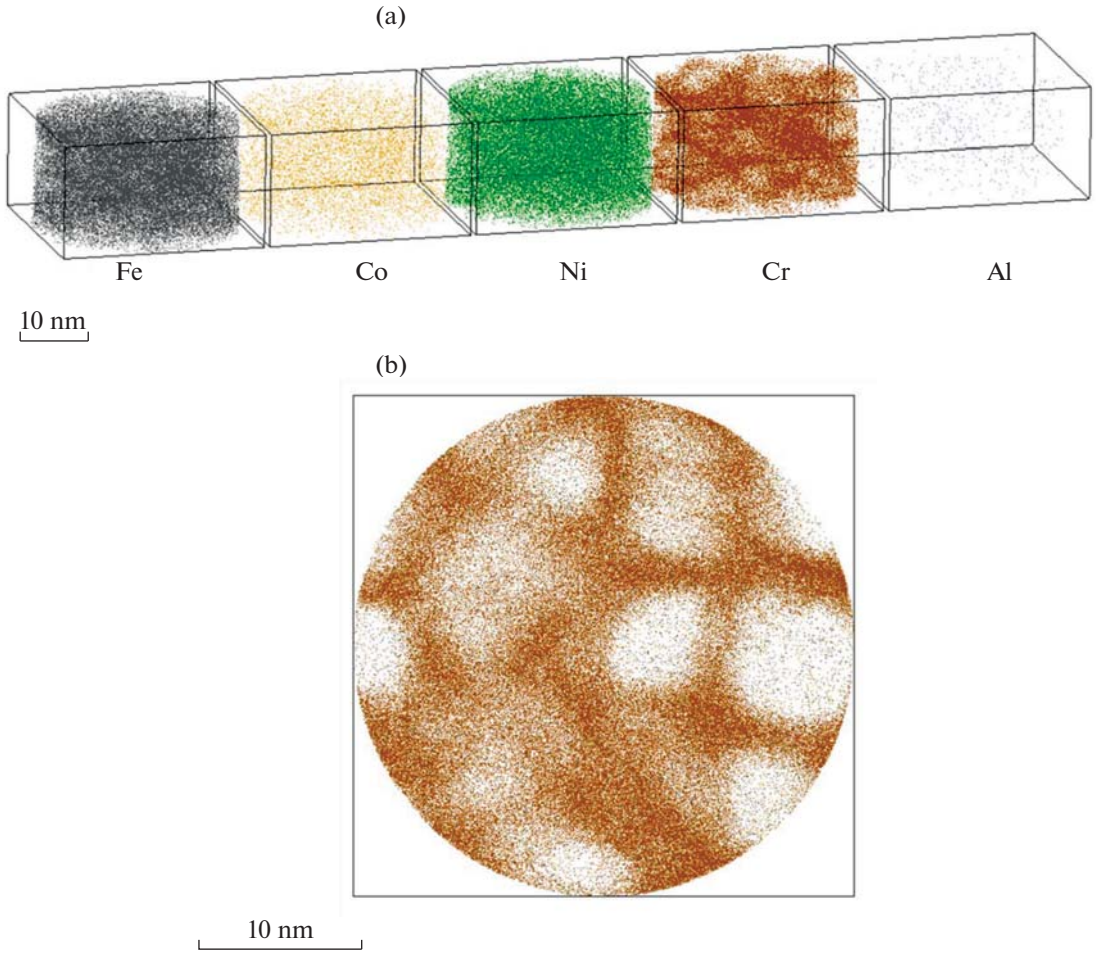

Fig. 3. Region of the Fe–Cr phase of AlCoCrFeNi HEA shown in Fig. 1B (A). Distribution of chromium in cross section 10 nm in thickness (B).

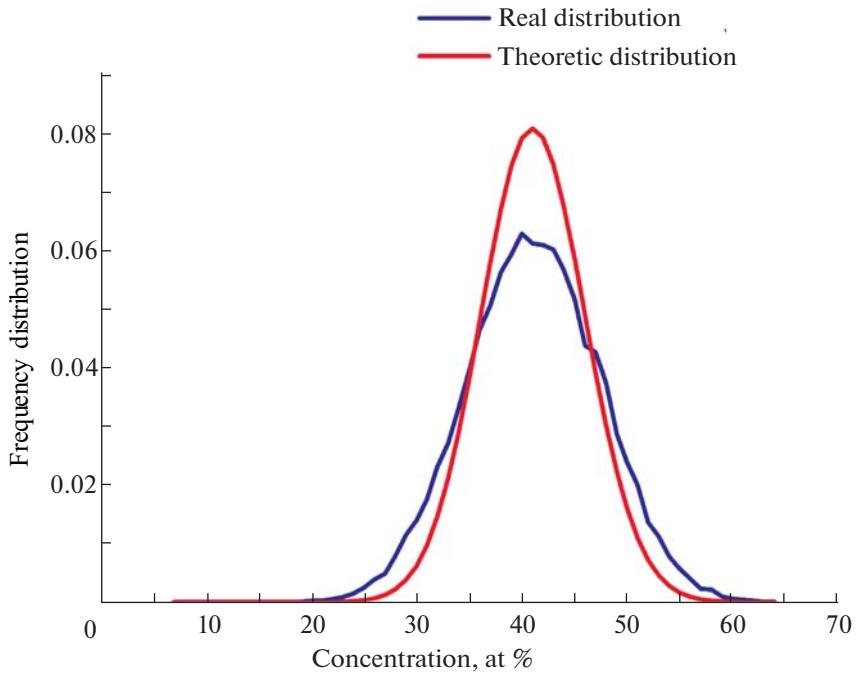

Fig. 4. Frequency distribution of chromium in the Fe–Cr phase of AlCoCrFeNi HEA (volume shown in Fig. 3).

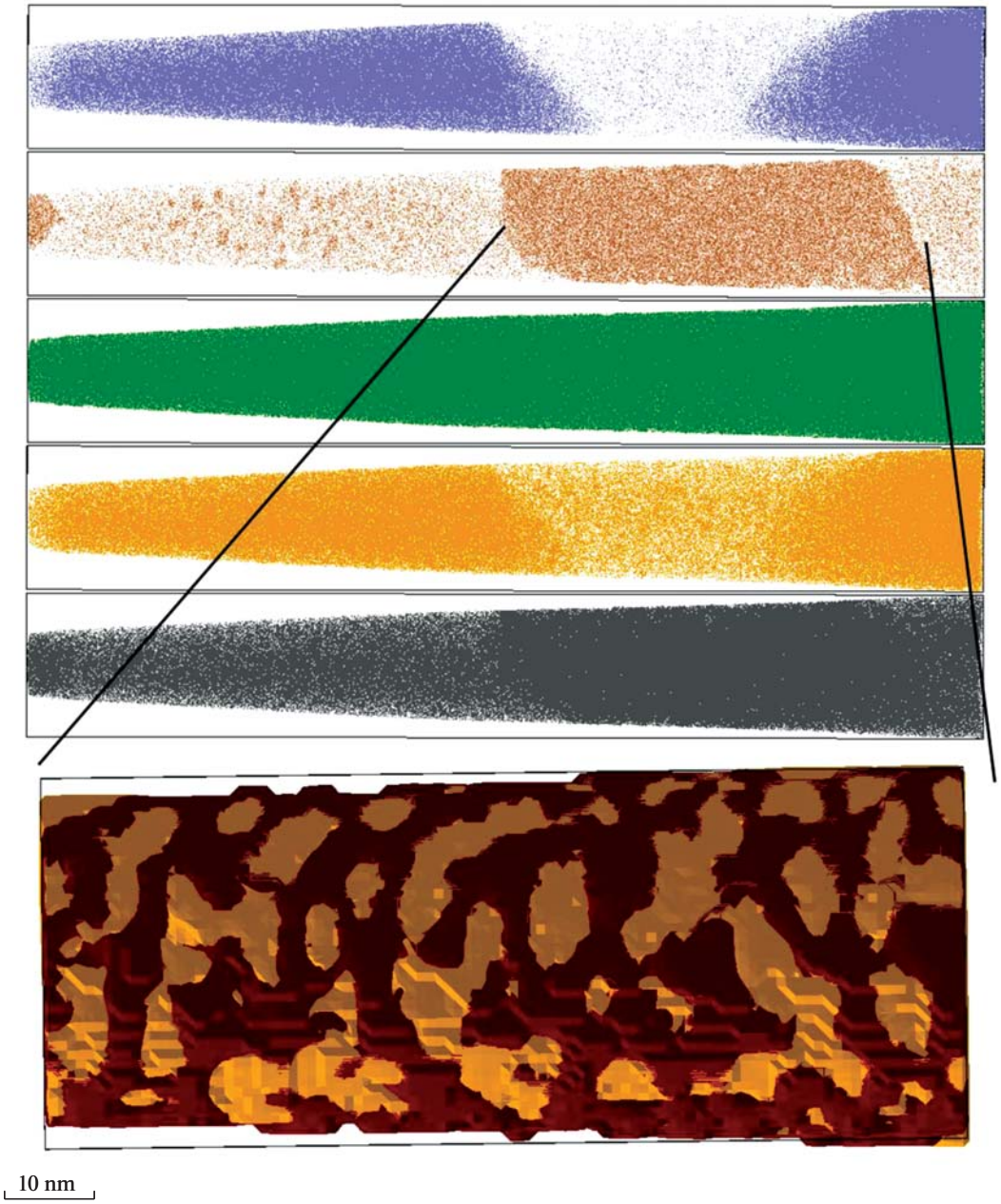

Fig. 5. Region of the Fe–Cr phase of AlCoCrFeNi HEA decorated with the cobalt isosurface (orange surface) with the concentration of 13.6 at %.

ment analysis, the "point-by-point" method, and the method of constructing isosurfaces and proxigrams (proxigram is an acronym for proximity histogram).

The frequency method is a statistical analysis of the distribution of atomic concentrations in the specimens of a certain size (usually one hundred atomic units). Theoretically, in a random solution, this distribution should take the form of a binomial distribution. In the case where there are several phase states in the volume under study, the frequency distribution contains sev-

Table 3. Mean chemical composition of the matrix and clusters in the Al–Ni phase (at %)

Element	Fe	Cr	Ni	Al	Co
Matrix	19.1 ± 0.9	4.6 ± 0.5	30 ± 2	24 ± 3	21.0 ± 0.7
Clusters	17 ± 3	50 ± 4	14 ± 4	8 ± 3	12 ± 2

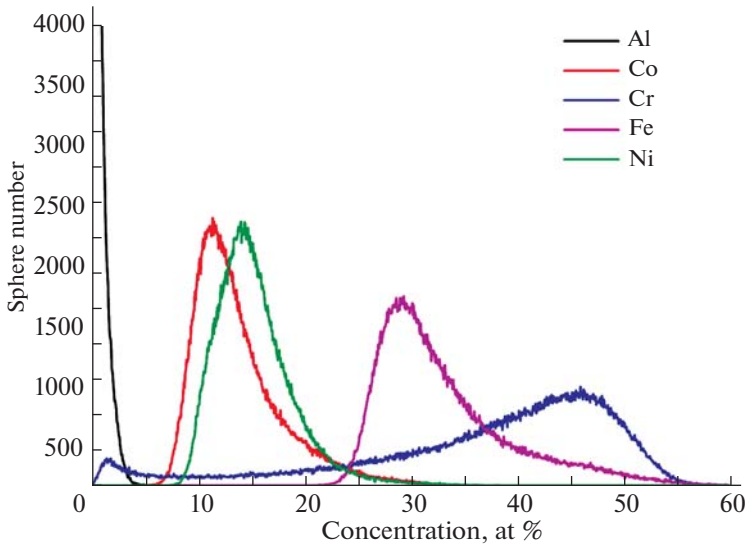

Fig. 6. Result of the analysis of the local chemical enrichment of the Fe–Cr phase of AlCoCrFeNi HEA (of the volume shown in Fig. 3).

eral local maxima corresponding to different phases of the material [25].

The method of local chemical analysis allows searching for areas enriched in a selected element and determining the mean values of concentrations of the chosen elements in the detected areas [26]. For this purpose, the concentrations of all elements are calculated in the given radius around each atom of the chosen type. On the basis of the obtained data, the concentration histogram is constructed for each element. If the element is distributed uniformly over the analyzed material, its histogram is represented by a single peak corresponding to the value of the mean concentration. A deviation of the real distribution, such as the peak displacement, indicates the nonuniform distribution of the chemical element over the volume. Several peaks indicate several stable phases in the volume.

The proxigram method [27] makes it possible to characterize the transition layer of the phase matrix for particles of arbitrary geometric shapes using the concentration profile. For this purpose, a supporting isoconcentration surface is constructed around the region under study. This closed surface confines the region where the concentration of a specific element (group of elements) is higher than the given one. The element (group of elements) is selected either visually from the atomic map, if possible, or after the preliminary procedures of integral structural-phase analysis (frequency methods, local chemical analysis method, etc.). In the first case, the concentration is selected so that the surface boundary coincides with the boundary of the visually identifiable enrichment region. In the second case, the concentration is chosen by the selection method. There are two aspects to consider when selecting the concentration. Firstly, it is necessary to exclude the presence of surfaces, whose appearance is caused by fluctuations in the concentrations of the chosen elements. Secondly, it is necessary to avoid fragmentation of the enrichment regions of interest into smaller surfaces. Hence, in the process of selection, the threshold concentration gradually increases until small (radius less than 1 nm) particles disappear and remaining large particles start to split into smaller ones. It is necessary to stop at the moment when the size and shape of large inhomogeneities stop changing significantly with a slight increase in the threshold concentration. The remaining surfaces become the reference ones for the proxigram method. This makes it possible to analyze the transition layer around each of these objects using a concentration profile, whose starting point is the corresponding surface. Concentration profiles are constructed in the direction perpendicular to the surface; they embrace the area inside and outside the enriched area. In order to achieve the best performance and required precision of the considered technique, the "marching cube" method is applied to construct the isosurface [28]. The obtained isosurface is smoothed using the "delocalization" algorithm [29] with the Epanechnikov kernel [30].

2. RESULTS OF THE ATOM PROBE TOMOGRAPHY EXAMINATIONS

The examples of atomic maps of the examined volumes are shown in Fig. 1. The images clearly show the regions that are depleted of or enriched in chromium and aluminum, which corresponds to different phases of the material. In confirmation of this, the frequency distribution of chromium (each block contains 100 atoms) is presented in Fig. 2, showing the presence of two phases with different contents of this element (~7 and 41 at %). Given these differences, we may say that

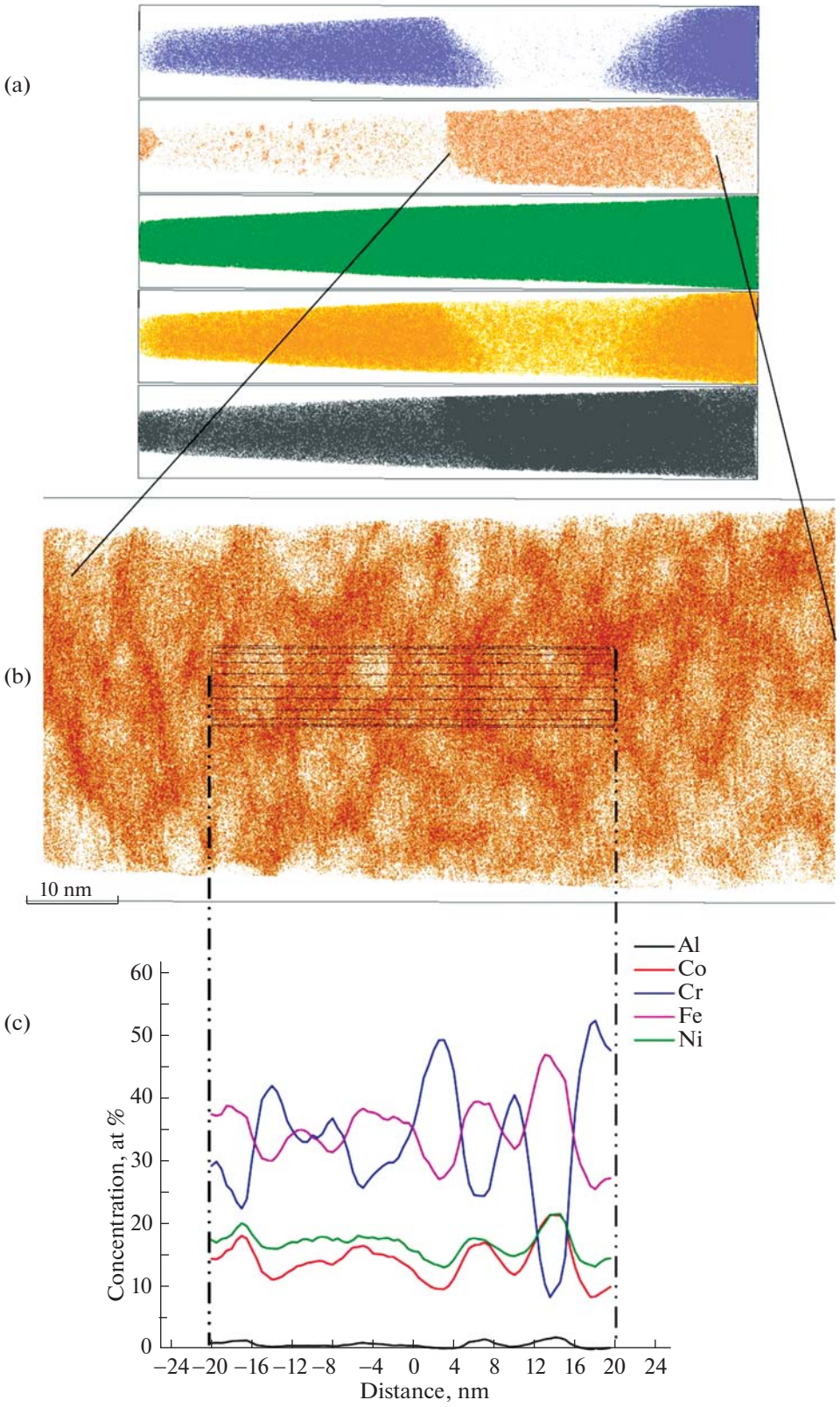

Fig. 7. Linear concentration profile (C) constructed for the region located in the Fe–Cr phase (A) cut out as a cylinder (B). The boundaries are shown by dashed lines.

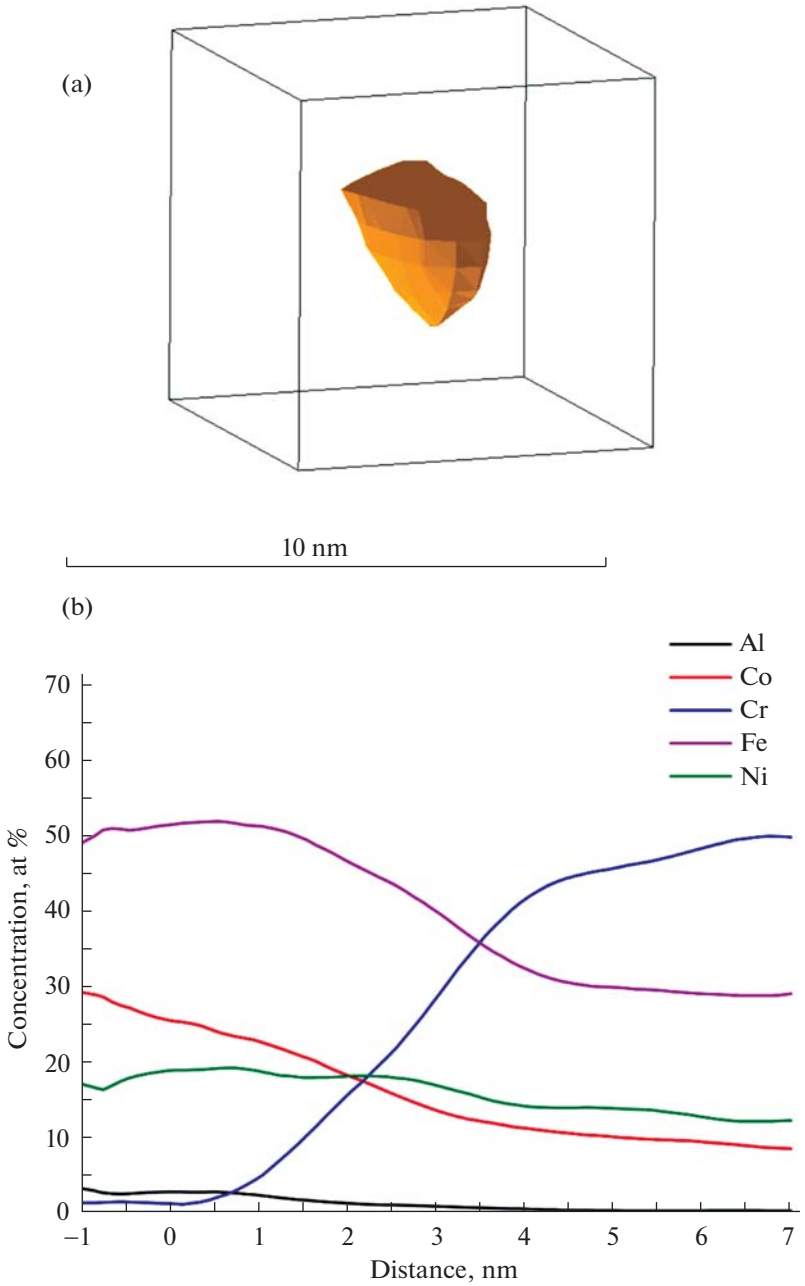

Fig. 8. Proxigram of a cobalt particle in the Fe–Cr phase of AlCoCrFeNi HEA. (A) Cobalt particle decorated with the isosurface with the reference concentration of 18.5 at % Co; (B) concentration profile constructed perpendicular to the isosurface (negative coordinate values show the inward direction in the particle, while positive values show the outward direction).

these are the enriched areas inside the dendrite or interdendrite phase [20]. The analysis of the chemical composition of these phases revealed that one of the phases was enriched in Cr and Fe, and the other was enriched in Ni and Al. The mean chemical composition of these phases is shown in Table 1.

It is noteworthy that the phase enriched in chromium is heterogeneous in its enrichment and contains nanoscale features in the form of regions enriched in chromium that surround the regions enriched in cobalt.

3.1. Analysis and Characterization of Fe–Cr Phase Features

The Fe–Cr phase is remarkable for its considerable chromium content, while the nickel and aluminum contents are low. However, as shown in Figs. 3A and 3B, chromium is distributed nonuniformly in this phase and forms a "honeycomb structure." Although this effect is easy to detect visually, the frequency diagram in Fig. 4 constructed for this phase does not show the apparent presence of two phases in the form

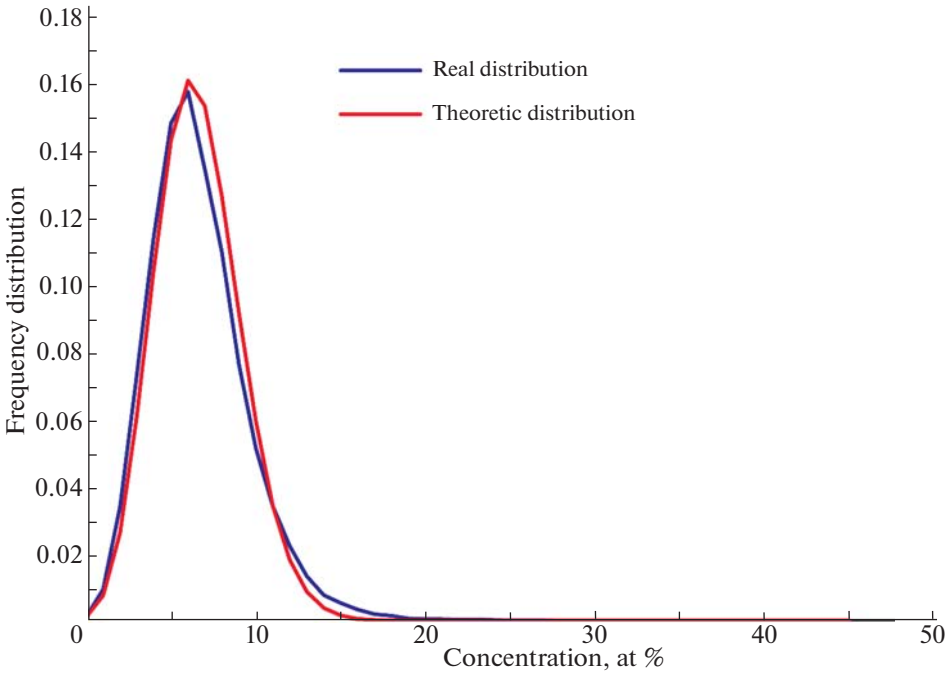

Fig. 9. Frequency chromium distribution in the Al–Ni phase of AlCoCrFeNi HEA (of the volume shown in Fig. 1B).

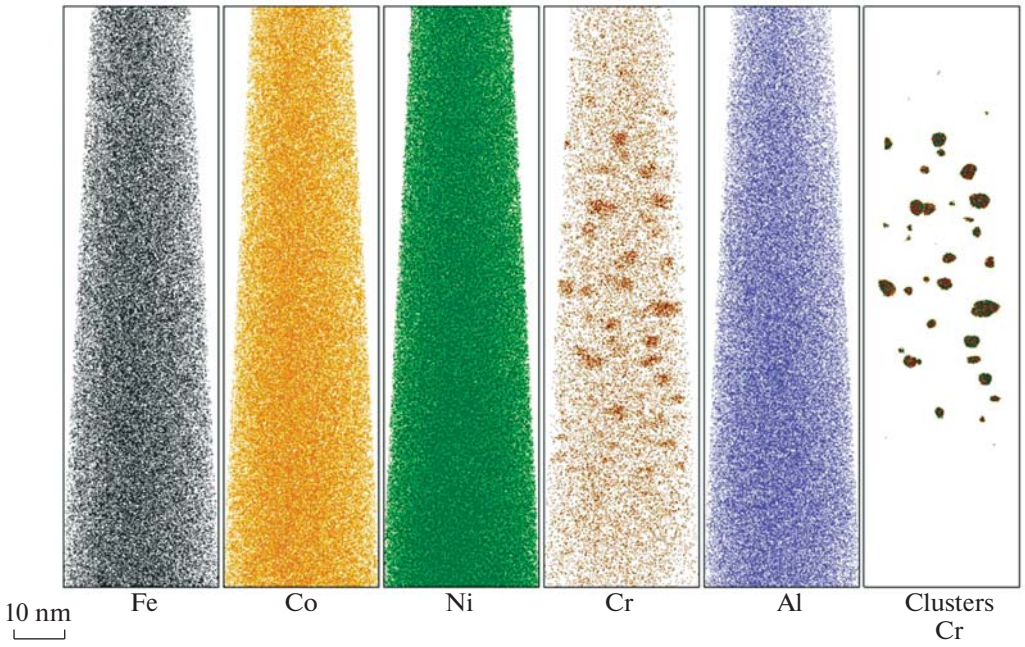

Fig. 10. Atomic map of the Al–Ni phase of AlCoCrFeNi HEA. For illustrative purposes, 10% of registered atoms are shown. The atomic map on the right shows regions with the Cr content larger than 37 at %.

of two separate peaks, but it only slightly differs in broadening from the theoretical distribution corresponding to a random volume distribution of chromium atoms. This fact indicates the necessity to characterize this phase using more precise methods, such as local chemical analysis. The isosurface analysis reveals that the Fe–Cr phase contains particles enriched in cobalt (see Fig. 5B). The results of the application of statistical methods demonstrating the presence of two stable states of chromium in this phase, in cobalt particles and in a honeycomb structure, are presented below. Figure 6 shows the results of analysis of the local chemical enrichment of the region under consideration. The analysis was performed by constructing spheres 1.2 nm in radius around cobalt atoms. The diagram shows the presence of two distinct

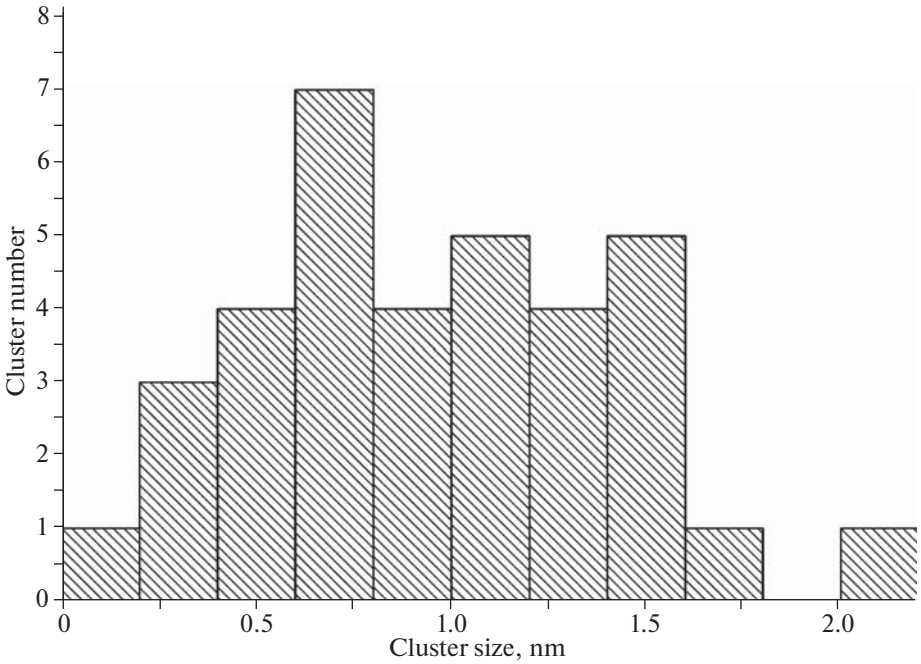

Fig. 11. Size distribution of clusters in the Al–Ni phase of AlCoCrFeNi HEA.

peaks of chromium, corresponding to approximately 2.5 and 50.0 at %. Hence, it should be noted that the Fe–Cr phase directly corresponds to the state with the chromium enrichment up to 50 at %, while in cobalt particles, which are located in the matrix of this phase, the chromium concentration decreases significantly. This is clearly shown by the linear concentration profile (Fig. 7C) constructed for the region confined by the cylinder (Fig. 7B) that embraces different features of the considered phase (Fig. 7A). The boundaries of the profile coincide with the boundaries of the cut-out region.

The complexity of the shape of cobalt particles does not allow their efficient characterization by radial or linear (Fig. 7) concentration profiles. The proxigram method, a rather new method for characterizing arbitrarily shaped precipitates, was applied for supplement and refinement. A particle shown in Fig. 8A is decorated by an isosurface constructed with the reference cobalt concentration of 18.5 at %, voxel grid size of 0.5 nm, and delocalization parameter of 2 nm. The concentration profile, a "proxigram," is constructed using this isoconcentration surface as shown in Fig. 7B.

It is shown in the figure that the chromium concentration that is typical of the considered phase decreases from 50 at % outside to a few atomic percent when approaching the center of the particle. In addition, the growth of nickel and aluminum concentrations should be noted, which is typical of the Al–Ni enriched phase, and the growth of iron concentration to 50 at %, which is not typical of this phase. Moreover, the cobalt concentration, initially lower than that of nickel, increases to 30% at the center of this particle, which exceeds the similar values in the Al–Ni phase. Table 2 presents the mean data for 39 particles that have been identified. This fact suggests that the identified precipitates are not residuals or seeds of the Al–Ni phase, but are unique objects of the system under consideration.

The analysis shows that there are strong anticorrelated fluctuations of Fe and Cr atoms in the Fe–Cr phase (see, for example, the profile constructed in Fig. 7A). In the regions a few nanometers wide, the local Fe concentration rises to 50 at % and Cr concentration grows to 50 at %. These opposite fluctuations, as well as the strongly intertwined morphology, are attributed to the spinodal decomposition of the phases enriched in Fe and Cr [31, 32].

3.2. Analysis and Characterization of the Al–Ni Phase Features

Although the chromium frequency distribution in the Al–Ni phase does not indicate any phase features (see Fig. 9), the analysis of the atomic map of this phase reveals nanoscale regions with increased chromium content (see Fig. 10). These inclusions have an almost spherical shape and can be identified using cluster search methods. The procedure of cluster search by the maximum separation method [33] with the following search parameters was used for their further characterization: search radius $r = 1$ nm, Cr concentration not less than 37 at % in the vicinity of radius r, and minimum cluster size of 100 atoms. The clusters with radii from 0.7 to 2.7 nm were found. The size distribution of the clusters is shown in Fig. 11. The mean

chemical composition is presented in Table 3. The volume density of the clusters is $(6 \pm 2) \times 10^{17}$ cm^{-3}.

CONCLUSIONS

In this paper, an alloy of the AlCoCrFeNi type was studied. The newest precise methods of atom probe data analysis were applied, which made it possible to carry out a detailed study of the main phase components and the precipitates of other phases inside the main phases. In the volumes studied, the phases enriched either in Fe and Cr or in Al and Ni were found. These phases form a considerable share of the investigated volumes and their sizes exceed hundreds of nanometers. Inside the Fe–Cr phase, particles enriched in Fe and Co were found. Their size was ~10 nm. The analysis showed that, in the detected particles, Cr was replaced with Co and Fe atoms, whose concentration increased by 3 and 1.5 times, respectively, compared with the concentration in the matrix. The Fe and Co concentrations increased with the approach to the center of the identified particles. Inclusions enriched in Fe and Cr were found inside the Al–Ni phase. The composition of these particles coincided with that of the Fe–Cr phase matrix, which suggested that they might be seeds of this phase inside the Al–Ni phase. The volume density of the identified clusters was $(6 \pm 2) \times 10^{17}$ cm^{-3}.

FUNDING

This work was supported by the Russian Foundation for Basic Research, project no. 18-38-00859. The atom probe tomography examinations were performed at the KAMIKS Shared Access Center (http://kamiks.itep.ru/) at the Alikhanov Institute for Theoretical and Experimental Physics, National Research Center Kurchatov Institute.

REFERENCES

1. J.-W. Yeh, S.-K. Chen, S.-J. Lin, J.-Y. Gan, T.-S. Chin, T.-T. Shun, C.-H. Tsau, and S.-Y. Chang, Adv. Eng. Mater. **6**, 299 (2004).
2. B. Cantor, I. T. H. Chang, P. Knight, and A. J. B. Vincent, Mater. Sci. Eng. A **375–377** (2004).
3. J.-W. Yeh, J. Miner. Met. Mater. Soc. **67**, 2254 (2015).
4. K.-Y. Tsai, M.-H. Tsai, and J.-W. Yeh, Acta Mater. **61**, 4887 (2013).
5. T. Egami, W. Guo, P. D. Rack, and T. Nagase, Metall. Mater. Trans. A **45**, 180 (2014).
6. S. J. Zinkle and L. L. Snead, Ann. Rev. Mater. Res. **44**, 241 (2014).
7. G. A. Salishchev, M. A. Tikhonovsky, D. G. Shaysultanov, N. D. Stepanov, A. V. Kuznetsov, I. V. Kolodiy, A. S. Tortika, and O. N. Senkov, J. Alloys Compd. **591**, 11 (2014).
8. A. Gali and E. P. George, Intermetallics **39**, 74 (2013).
9. M. Kang, J. W. Won, J. B. Kwon, and Y. S. Na, Mater. Sci. Eng. A **707**, 16 (2017).
10. B. Gludovatz, A. Hohenwarter, D. Catoor, E. H. Chang, E. P. George, and R. O. Ritchie, Science (Washington, DC, U. S.) **345** (6201), 1153 (2014).
11. M. A. Hemphill, T. Yuan, G. Y. Wang, J. W. Yeh, C. W. Tsai, A. Chuang, and P. K. Liaw, Acta Mater. **60**, 5723 (2012).
12. M.-H. Chuang, M. H. Tsai, W.-R. Wang, S.-J. Lin, and J.-W. Yeh, Acta Mater. **59**, 6308 (2011).
13. C. J. Tong, M. R. Chen, S. K. Chen, J. W. Yeh, T. T. Shun, S. J. Lin, and S. Y. Chang, Metall. Mater. Trans. A **36A**, 1263 (2005).
14. J. W. Yeh, Y. L. Chen, S. J. Lin, and S. K. Chen, in *Advanced Structural Materials,* Ed. by H. B. Ramirez, J. G. Cabanas-Moreno, H. A. Calderon-Benavides, K. Ishizaki, and A. Salinas Rodriguez (2007), Vol. 3, p. 1.
15. S. Singh, N. Wanderka, B. S. Murty, and U. Glatze, Intermetallics **59**, 182 (2011).
16. C. M. Lin and H. L. Tsai, Intermetallics **19**, 288 (2011).
17. T. T. Shun and Y. C. Du, J. Alloys Compd. **479**, 157 (2009).
18. Y. P. Wang, B. S. Li, M. X. Ren, C. Yang, and H. Z. Fu, Mater. Sci. Eng. A **491**, 154 (2008).
19. T. T. Shun, C. H. Hung, and C. F. Lee, J. Alloys Compd. **495**, 55 (2010).
20. Y. Linden, M. Pinkas, A. Munitz, and L. Meshi, Scr. Mater. **139**, 49 (2017).
21. S. V. Rogozhkin, A. A. Aleev, A. A. Lukyanchuk, A. S. Shutov, O. A. Raznitsyn, and S. E. Kirillov, Instrum. Exp. Tech. **60**, 428 (2017).
22. A. A. Aleev, S. V. Rogozhkin, A. A. Luk'yanchuk, A. S. Shutov, O. A. Raznitsyn, A. A. Nikitin, N. A. Iskandarov, O. A. Korchuganova, and S. E. Kirillov, State Registration Certificate of Computer Program No. 2018661876 (2018).
23. O. A. Raznitsyn, A. A. Lukyanchuk, A. S. Shutov, S. V. Rogozhkin, and A. A. Aleev, J. Anal. Chem. **72**, 1404 (2017).
24. M. K. Miller, *Atom Probe Tomography: Analysis at the Atomic Level* (Kluwer Academic, New York, 2000).
25. T. J. Godfrey, M. G. Hetherington, J. M. Sassen, and G. D. W. Smith, J. Phys. (Paris) **49** (C6), 421 (1988).
26. J. M. Hyde, A. Cerezo, and T. J. Williams, Ultramicroscopy **109**, 502 (2009).
27. B. Gault and M. P. Moody, Springer Ser. Mater. Sci. **160**, 240 (2012).
28. W. E. Lorensen and H. E. Cline, Comput. Graphics **21**, 163 (1987).
29. B. Gault and M. P. Moody, Springer Ser. Mater. Sci. **160**, 233 (2012).
30. V. A. Epanechnikov, Theory Prob. Appl. J. **14**, 153 (1969).
31. M. K. Miller and E. A. Kenik, Microsc. Microanal. **10**, 336 (2004).
32. M. K. Miller, J. M. Hyde, M. G. Hetherington, A. Cerezo, G. D. W. Smith, and C. M. Elliott, Acta Metall. Mater. **43**, 3385 (1995).
33. A. Manzoni, H. Daoud, R. Völkl, U. Glatzel, and N. Wanderka, Ultramicroscopy **132**, 212 (2013).

Translated by N. Semenova

SPELLOK